HHS Public Access

Author manuscript

Nat Methods. Author manuscript; available in PMC 2015 January 01.

Published in final edited form as:

Nat Methods. 2014 July ; 11(7): 727–730. doi:10.1038/nmeth.2964.

Simultaneous whole-animal 3D-imaging of neuronal activity using light-field microscopy

Robert Prevedel[#1,2,3], **Young-Gyu Yoon**[#4,5], **Maximilian Hoffmann**[1,2,3], **Nikita Pak**[5,6], **Gordon Wetzstein**[5], **Saul Kato**[1], **Tina Schrödel**[1], **Ramesh Raskar**[5], **Manuel Zimmer**[1], **Edward S. Boyden**[5,7,8,9], and **Alipasha Vaziri**[1,2,3]

[1]Research Institute of Molecular Pathology, Vienna, Austria

[2]Max F. Perutz Laboratories, University of Vienna, Vienna, Austria

[3]Research Platform Quantum Phenomena & Nanoscale Biological Systems (QuNaBioS), University of Vienna, Austria

[4]Department of Electrical Engineering and Computer Science, Massachusetts Institute of Technology (MIT), Cambridge, MA, USA

[5]MIT Media Lab, Massachusetts Institute of Technology (MIT), Cambridge, MA, USA

[6]Department of Mechanical Engineering, Massachusetts Institute of Technology (MIT), Cambridge, MA, USA

[7]Department of Biological Engineering, Massachusetts Institute of Technology(MIT), Cambridge, MA, USA

[8]Department of Brain and Cognitive Sciences, Massachusetts Institute of Technology (MIT), Cambridge, MA, USA

[9]McGovern Institute, Massachusetts Institute of Technology (MIT), Cambridge, MA, USA

[#] These authors contributed equally to this work.

Abstract

High-speed large-scale 3D imaging of neuronal activity poses a major challenge in neuroscience. Here, we demonstrate intrinsically simultaneous functional imaging of neuronal activity at single neuron resolution for an entire *Caenorhabditis elegans* as well as for the whole-brain of larval zebrafish. Our technique captures dynamics of spiking neurons in volumes of ~700 μm x 700 μm x

Correspondence should be addressed to E.S.B. (esb@media.mit.edu) or A.V. (vaziri@imp.ac.at)..

AUTHOR CONTRIBUTIONS

R.P. designed microlenses, built imaging system and performed experimentstogether with M.H. Y.-G.Y. designed and wrote 3D-deconvolution software withcontributions from G.W under the guidance of R.R. R.P. and M.H. refined andrebuilt the imaging system and analyzed data together with Y.-G.Y; N.P.implemented and tested LFDM prototype; T.S. generated transgenic animals,provided microfluidic devices and performed cell identifications under theguidance of M.Z., S.K. wrote analysis software. E.S.B. and A.V. conceived and ledproject. R.P., Y.-G.Y. and A.V. wrote the manuscript, with input from all authors.

COMPETING FINANCIAL INTERESTS

The authors declare no competing financial interests.

200 μm at 20 Hz and its simplicity makes it an attractive tool for high-speed volumetric calcium imaging.

To understand how sensory inputs are dynamically mapped onto functional activity of neuronal populations and how their processing leads to cognitive functions and behavior, tools for non-invasive interrogation of neuronal circuits with high spatio-temporal resolution are required [1, 2]. A number of approaches for 3D neural activity imaging, taking advantage of chemical and genetically encoded fluorescent reporters [3,4] exist. While some or are based on scanning the excitation light in a volume, either sequentially [5-7] or randomly [8, 9], others try to capture 3D image data simultaneously by mapping axial information onto a single lateral plane using a range of approaches [10-14].

Light-field microscopy (LFM) [12] is one such simultaneous 3D imaging method which has been applied to still and *in-vitro* biological samples [12, 13]. In contrast to conventional imaging schemes a light-field microscope captures both the 2D location and 2D angle of the incident light. This is done by placing a microlense array in the native image plane such that sensor pixels capture the rays of the light-field simultaneously. Such 4D light-fields allow the synthesis of a focal stack computationally. Since in LFM single sensor images are used to retrieve the entire 3D volume information, this enables high-speed volumetric acquisition. However, to date, despite its potentially superb temporal resolution, LFM has not been used for any functional biological imaging. This is because capturing the 4D light-field information by a single senor image comes at the cost of reduced spatial resolution and inherent trade-offs between axial imaging range and the spatial and axial resolution[12].

Here, we report that neural systems equipped with calcium sensors can be imaged at volume rates of up to 50 Hz and at single neuron resolution, using a 3D deconvolution algorithm 15, 16 applied to LFM. We achieve effective resolutions up to ~1.4 μm and 2.6 μm in the lateral and axial dimensions respectively, inside biological samples. Using Caenorhabditis elegans we demonstrate simultaneous recording of neuronal population activity over a field of view (FOV) of ~350 μm × 350 μm × 30 μm sufficient to capture the dynamics of neurons distributed across its entire nervous system. In particular, we show that the activity of the majority of head ganglia neurons can be recorded simultaneously with selected neurons in the ventral cord. Further, by performing whole-brain Ca^{2+} imaging in live zebrafish larvae we demonstrate the ability of our technique to capture dynamics of spiking neurons in volumes as large as ~700 μm × 700 μm × 200 μm at 20 Hz. Our light-field deconvolution microscope (LFDM) can be easily integrated into any epi-fluorescence microscope and provides a simple and costeffective approach to obtain high-speed volumetric imaging capabilities.

To realize a LFDM, we placed a microlens array at the image plane of an epifluorescence microscope (**Fig. 1a** and Methods), which captured the different perspectives of the sample (**Fig. 1b**) on the camera sensor. To overcome the trade-off between axial and lateral spatial resolution in LFM [12] we exploited aliasing of the recorded data and used computational reconstruction methods based on 3D-deconvolution to effectively obtain improved lateral and axial resolution 15, 16 (see Methods and **Supplementary Note 1 & 2** for details).

To evaluate the spatial resolution of our LFDM we imaged sub-diffraction beads and reconstructed the point-spread function (PSF) of our system (**Fig. 1b-c**). Using a 40× objective we found a resolution of ~1.4 μm (2.6 μm) in the lateral (axial) dimension. To verify the suitability of LFDM for capturing the activity of individual neurons, we imaged a sample consisting of 6 μm-sized fluorescent beads randomly distributed in three dimensions in agarose and compared a conventional focal stack (taken without microlenses) (**Fig. 1d-e**) with the deconvolved light-field images (**Fig. 1f-g**).

Using the same objective we were able to image the majority of *C. elegans* (~350 μm x 350 μm x 30 μm) while maintaining single-neuron resolution (**Fig. 2a-c; Supplementary Fig. 1-4** and **Supplementary Video 1-5**). We could record activity of neurons in the brain region surrounding the nerve ring and the ventral cord at 5 Hz volume rate. We note that our LFDM allows for substantially higher volume rates which we demonstrated by recording unrestrained worms at 50 Hz (**Supplementary Fig. 4** and **Supplementary Video 3**). Such volume rates would in principle be sufficient for performing whole brain imaging in freely moving worms, especially if additional tracking is employed as previously shown for single neurons 17. However, since Ca^{2+}-signals in *C. elegans* occur typically at timescales of up to 1 Hz, we chose slower volume rates (5 Hz) in order to maximize signal-to-noise and reduce potential photo-bleaching. The wide FOV of LFDM and the intrinsic simultaneity of the acquisition allow to study correlations in activity of far-away neurons, which would not be feasible with other unbiased Ca^{2+}-imaging techniques. In our experiments, we observed correlated and anti-correlated activity patterns between the pre-motor interneurons in the head and motor neurons located along the ventral nerve cord, which connect to body wall muscles according to the wormatlas (**Fig. 2a-c**). Additionally, the location, morphology and the neuronal activity patterns of some of these neurons allowed us to identify specific pre-motor interneuron classes such as AVA, AVE, RIM, AIB, AVB and A- and B-class motor neurons, that have been associated with motor program selection (**Supplementary Fig. 3**) [18]. AVA neurons have been associated with a switch from forward to backward directed crawling, which depends on A-class motor neurons [19], and is associated with a change in the relative activities of A- and B-class motorneurons [18]. Consistent with these findings, we observed a high level of correlation of AVA and A-class motor neuron activity and an anti-correlation in the activity of AVA with B-class motor neuron. Further, we demonstrated that sensory stimulation can be used to identify neuron classes (**Supplementary Fig. 3**). Morphology, location and activity patterns of these neuron classes match with those of the oxygen chemosensory neurons BAG and URX [5].

We also recorded exclusively from brain regions surrounding the nerve ring (**Fig. 2d-f**, and **Supplementary Fig. 2)**. Imaging smaller FOVs (~200 μm x 70 μm x 30 μm) leads to faster volume reconstructions and less artifacts stemming from brightly fluorescing cells, such as coelomocytes. Similar to previous findings [5], we were able to resolve up to 74 individual neurons in a typical recording, of which around 30 showed pronounced activity over the recording time of 200 seconds (**Fig. 2d-f**, and **Supplementary Fig. 2).**

In order to highlight the temporal resolution and the broader applicability of our technique we performed Ca^{2+}-imaging in live zebrafish larvae brains expressing GCaMP5 pan-neuronally. Employing a 20× objective, we demonstrated wholebrain Ca2+ imaging for

volumes spanning ~700 μm × 700 μm × 200 μm at a 20 Hz volume rate. Although in this case optical single-cell resolution had to be compromised in favor of larger FOVs, spatially resolved cellular signals over the entire time series could still be recovered using standard signal extraction and unmixing techniques [20]. Implementing this approach we could extract neuronal activity for ~5000 cells across the brain, and follow their fast Ca2+-transients on millisecond timescale (**Fig. 3** and **Supplementary Video 6).** In particular, by applying an aversive odor to the fish we could evoke neuronal activity and infer dynamics of Ca^{2+}-signals across the olfactory system, the midbrain and parts of the hindbrain consistent with previous demonstrations of the neuronal dynamics in these regions [6, 7, 21-23]. Our imaging speed, more than an order of magnitude faster than in previous whole-brain functional imaging demonstrations [6, 7], is thus able to reliably capture the dynamic activity of a large number of cells with high spatial and temporal resolution.

In summary, we have implemented a LFDM and demonstrated its ability to simultaneously capture the neuronal activity of the entire nervous system of *C. elegans* at single cell resolution as well as record dynamics of spiking neurons by performing whole-brain Ca+*2* imaging in larval zebrafish at 20 Hz. The increase in spatial resolution compared to LFM was achieved by performing deconvolution during post-processing. The simultaneity of acquisition of volumes in LFDM eliminates spatio-temporal ambiguity associated with sequentially recorded approaches and decouples temporal resolution from volume size. Resolutions in all three dimensions are set by the objective and microlens properties, while FOV and acquisition rate are determined by the camera chip size, frame rates and signal intensity. LFDM is easy to set-up, cost-effective and compatible with standard microscopes. In addition, both the temporal resolution and the obtainable FOVs, make LFDM an attractive technique for future combination with behavioral studies. Thus, we expect that LFDM will find rapid and widespread use within the neuroscience community. Future work will focus on obtaining higher spatial resolutions and larger FOVs as well as faster and more efficient computational reconstruction techniques, both of which of are expected to improve with technological advancements in camera sensors and processors. Finally, the use of red-shifted Ca^{2+}-sensors [24] and the combination of LFDM with techniques for imaging at depth in biological tissue [25] bears further potential for wide-spread use of this method.

Online Methods

Setup

The LFM system is appended to an epi-fluorescence microscope (Zeiss, Axiovert200) equipped with a LED excitation light source (λ = 488nm, 300 mW, CoolLED)and a standard GFP filter set (Zeiss). In all *C. elegans* imaging experiments, weused a 40× 0.95NA dry objective (Zeiss APOCHROMAT), while zebrafish imagingwas performed with a 20x 0.5NA dry objective (Zeiss Plan-NEOFLUAR). Themicrolens array is mounted inside a 5-axis kinematic mount (Thorlabs) to allowfine adjustment of the array orthogonal to the optics axis, which we found crucialfor high-quality results. The array is further imaged onto a 5.5 Megapixel (2560 x2160 pixels) sCMOS camera (Andor Zyla) utilizing a 1:1 relay macro lensobjective (Nikon AF-S 105mm 2.8 G VR IF-ED Micro) (**Fig. 1a**). Details on opticaldesign choices and their effect on resolution are discussed in **Supplementary Note 1.**

C. elegans experiments

To record neuronal activity from *C. elegans*, we loaded adult worms (one- tofour-egg-stage) expressing nls-GCaMP5K under the *punc31*-promoter (strainsZIM294 and ZIM617) into a microfluidic channel which was connected to areservoir containing S-Basal buffer with 5 mM tetramisole, an acetylcholinereceptor–specific agonist that mildly paralyzes the animal's muscles to reducemotion [5]. The worm was placed off the native focal plane and towards the objective using a piezo stepper motor (PI-721, Physik Instrumente GmbH), suchthat the entire worm was ideally contained in the region spanning -30 μm to 0μm. By doing so we exploited the highest resolution of LFDM while avoidingartifacts near the focal plane. When recording from the head region only, theworm's head ganglia were placed at the center of the FOV and excitation waslimited to this area by the use of an iris in the excitation pathway. For the experiments involving chemosensory stimulation, we followed the procedure described in ref. 5.

Zebrafish larvae experiments

For zebrafish experiments, mit*f*α–/– larvae with pan-neuronal GCaMP5 expression have been imaged 5-8 dpf (days post fertilization) using stable lines *HuC:GCaMP5G* and *HuC:Gal4/UAS:GCaMP5G*, respectively. The fish wereimmobilized by embedding them in 2% agarose with their mouth and tailcleared of agarose to allow for odor stimulation and tail movement. Odorstimulation was performed by manually supplying water containing highly concentrated rotten fish extract into the imaging chamber during recordings.

Light-field deconvolution

The volume reconstruction itself can be formulated as a tomographic inverseproblem [26], where multiple different perspectives of an 3D volume are observed,and linear reconstruction methods–implemented via deconvolution–areemployed for computational 3D volume reconstruction. The image formation inlight-field microscopes involves diffraction from both the objective andmicrolenses. Point spread functions for the deconvolution can be computed fromscalar diffraction theory [27]. More details are given in **Supplementary Note 2.** After recording the raw light-field images, the digital images were cropped toregions of interest and resampled to contain 11 × 11 or 15 × 15 angular lightfieldsamples under each lenslet. Two calibration images, one showing themicrolenses with collimated rear-illumination and one showing a uniformfluorescent slide, were used for digital image rectification, in which camerapixels are assigned to individual microlenses. Reconstruction of each frame of animage sequence took between 2 and 30 minutes, depending on the size of theimage, number of iterations of the deconvolution algorithm, reconstruction method and workstation used. Computational resources are further discussed in **Supplementary Note 2.**

Ca^{2+} imaging data analysis

To extract a fluorescence time series for individual neurons from the 4D data,different strategies were employed for *C. elegans* and zebrafish. For *C. elegans*,we first applied rigid-body motion correction to each individual *z* plane movie.We then computed a median-intensity projection through time for each motioncorrectedz plane movie and used a maxima-finding algorithm to identify areas of peaked intensity in each projection. A circular

region of interest (ROI) wascreated surrounding each intensity peak, and overlapping ROI areas within *z* planes were eliminated. ROIs in adjacent *z* planes within an *x*-*y* distance of 7pixels were considered to be a component of the same neuron, up to a maximumof 5 planes, and for each neuron at each time point, the brightest 100 pixels ofthe aggregate of all pixels within the neuron's component ROIs were averaged toproduce a single fluorescence value and de-trended with an exponential decay function to account for photobleaching. For zebrafish, the data was first detrendedbased on the overall intensity of each frame. Then, to reduce time seriesdata, first in-active voxels were discarded based on their time-domain variance.Splitting the volume into smaller sub-volumes further reduced data size. We followed the strategy proposed in reference [20] to extract cellular signals from theCa^{2+}-imaging data. Each sub-volume data underwent PCA/ICA for automated spatial filter extraction where ideally each spatial filter corresponds to thelocation of a neuron [20]. After automatically rejecting spatial filters based on sizeand dispersion, we applied the spatial filters to the 4D data to extract their fluorescence intensity. Time-points during which the fish seemed to contract where discarded and replaced with nearest neighbor fluorescence intensities.These contractions typically lasted between 200 ms and 1 sec only and weretemporally very sparse. Therefore we regarded them negligible compared to the overall recording time. Fish which moved substantially during image acquisitionwere discarded from analysis. To extract $\Delta F/F_0$, we calculated $\Delta F/F_0 = 100 * (F_{(t)} - F_0)/F_0$, with F_0 being the mean fluorescence intensity of each corrected trace.

Supplementary Material

Refer to Web version on PubMed Central for supplementary material.

ACKNOWLEDGMENTS

We thank T. Müller, P. Pasierbek, P. Forai, H. Kaplan, M. Molodtsov, K. Tessmar-Raible and F. Schlumm for technical support and loan of equipment, as well as H.Baier (MPL for Neurobiology, Munich) and M. Orger (Champalimaud, Lisbon) forsharing zebrafish lines. The computational results presented have been achievedin part using the Vienna Scientific Cluster (VSC). R.P. acknowledges the VIPSProgram of the Austrian Federal Ministry of Science and Research and the City ofVienna as well as the European Commission (Marie Curie, FP7-PEOPLE-2011-IIF). Y.-G.Y. was supported by Samsung Scholarship. N.P. was supported by anNSF Graduate Fellowship. ESB was supported by the Allen Institute for BrainScience, the MIT Media Lab, the MIT McGovern Institute, NIH 1R01EY023173,the MIT Synthetic Intelligence Project, the IET Harvey Prize, NSF CBET 1053233,the New York Stem Cell Foundation-Robertson Award, NSF CBET 1344219, NIH1DP1NS087724, Google, the NSF Center for Brains Minds and Machines at MIT,and Jeremy and Joyce Wertheimer. The research leading to these results hasreceived funding from the Vienna Science and Technology Fund (WWTF) projectVRG10-11, Human Frontiers Science Program Project RGP0041/2012, ResearchPlatform Quantum Phenomena and Nanoscale Biological Systems (QuNaBioS)and Research Institute of Molecular Pathology (IMP). M.Z. and T.S. receivedfunding from the European Community's Seventh Framework Program(FP7/2007-2013)/ERC grant agreement no. 281869 – *elegansNeurocircuits*. TheIMP is funded by Boehringer Ingelheim.

REFERENCES

1. Alivisatos AP, et al. Neuron. 2012; 74:970–974. [PubMed: 22726828]
2. Marblestone AH, et al. Front. Comput. Neurosci. 2013; 7:34. [PubMed: 23596412]
3. Stosiek C, Garaschuk O, Holthoff K, Konnerth A. Proc Natl Acad Sci U S A. 2003; 100:7319–7324. [PubMed: 12777621]
4. Chen T-W, et al. Nature. 2013; 499:295–300. [PubMed: 23868258]

5. Schrodel T, Prevedel R, Aumayr K, Zimmer M, Vaziri A. Nature Methods. 2013; 10:1013–1020. [PubMed: 24013820]
6. Ahrens MB, Keller PJ. Nature Methods. 2013; 10:413–420. [PubMed: 23524393]
7. Panier T, et al. Frontiers in neural circuits. 2013; 7:65. [PubMed: 23576959]
8. Reddy GD, Kelleher K, Fink R, Saggau P. Nat. Neurosci. 2008; 11:713–720. [PubMed: 18432198]
9. Grewe BF, Langer D, Kasper H, Kampa BM, Helmchen F. Nature Methods. 2010; 7:399–391. [PubMed: 20400966]
10. Cheng A, Goncalves JT, Golshani P, Arisaka K, Portera-Cailliau C. Nature Methods. 2011; 8:139–158. [PubMed: 21217749]
11. Abrahamsson S, et al. Nature Methods. 2013; 10:60–80. [PubMed: 23223154]
12. Levoy M, Ng R, Adams A, Footer M, Horowitz M. ACM Trans. Graph. 2006; 25:924–934.
13. Levoy M, Zhang Z, McDowall IJ. Microsc. 2009; 235:144–162.
14. Quirin S, Peterka DS, Yuste R. Optics Express. 2013; 21:16007–16021. [PubMed: 23842387]
15. Agard DA. Annual Review of Biophysics and Bioengineering. 1984; 13:191–219.
16. Broxton M, et al. Optics Express. 2013; 21:25418–25439. [PubMed: 24150383]
17. Faumont S, et al. PLoS One. 2011; 6:e24666. [PubMed: 21969859]
18. Kawano T, et al. Neuron. 2011; 72:572–586. [PubMed: 22099460]
19. Chalfie M, et al. The Journal of Neuroscience : the official journal of the Society for Neuroscience. 1985; 5:956–964. [PubMed: 3981252]
20. Mukamel EA, Nimmerjahn A, Schnitzer MJ. Neuron. 2009; 63:747–760. [PubMed: 19778505]
21. Friedrich RW, Korsching SI. Neuron. 1997; 18:737–752. [PubMed: 9182799]
22. Renninger SL, Orger MB. Methods. 2013; 62:255–267. [PubMed: 23727462]
23. Jetti, Suresh K.; Vendrell-Llopis, N.; Yaksi, E. Current biology. 2014; 24:434–439. [PubMed: 24508164]
24. Akerboom J, et al. Frontiers in Molecular Neuroscience 6 2. 2013
25. Ntziachristos V. Nature Methods. 2010; 7:603–614. [PubMed: 20676081]
26. Kak AC, Slaney M. Classics in Applied Mathematics. 2001 ISBN: 978-0-89871-494-4.
27. Gu M. Advanced Optical Imaging Theory *Springer*. 1999 ISBN-10: 981402130X.

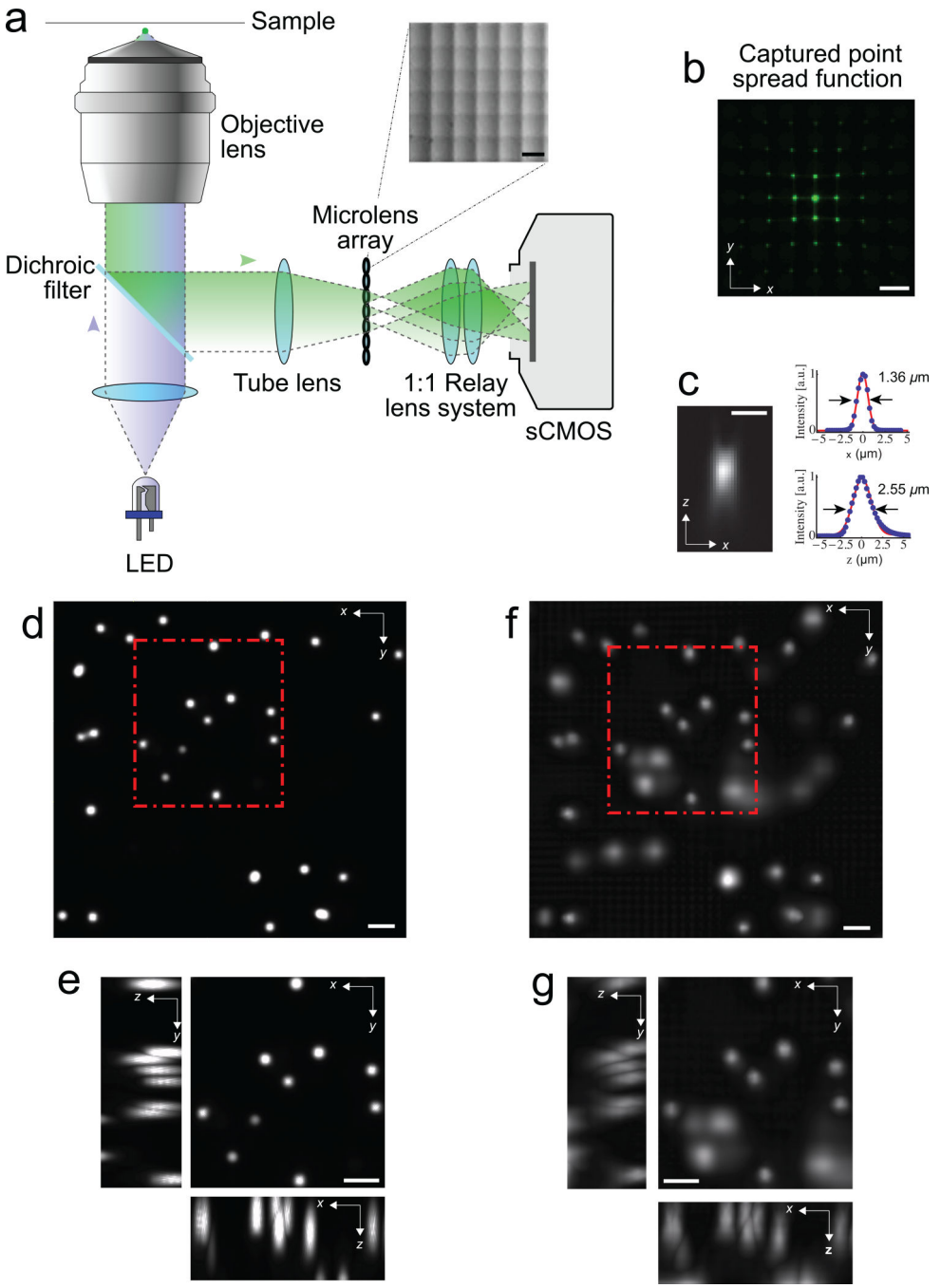

Figure 1.

Light-field deconvolution microscopy (LFDM). (**a**) A microlens arraywas appended to the camera port of a standard wide-field microscope. The lensarray (pitch 150 μm, focal length 3mm, OKO Tech) was placed in the primaryimage plane of the fluorescence microscope. The array itself was imaged with a1:1 relay lens system onto the chip of a sCMOS camera. See Methods for details.The inset shows a close-up picture of the microlens array. (**b**) The point spreadfunction (PSF) of a sub-diffraction sized bead located at $z = 7.5$ μm off the focalplane, as seen through the microlens array. Scale bar 150 μm in (**a, b**). (**c**) Axial(xz)

PSF at z = 7.5 μm, reconstructed using LFDM, and corresponding x- as wellas z-profiles, showing lateral and axial resolution, respectively. Scale bar 3 μm.(**d**) Maximum-intensity projection of a deconvolved wide-field focal stack taken without microlenses. The sample consists of 6 μm-sized fluorescent beads inagarose, mimicking the distribution of neurons in *C. elegans*. (**e**) Zoom-in of highlighted area, with xz- as well as yz-section maximum-intensity projections.The individual beads are well resolved in this image. (**e, f**) Correspondingvolume of the same beads, 4 – 28 μm off the focal plane, reconstructed via 15iterations of light-field deconvolution algorithm. Although the fluorescence ofsome lower lying beads is faintly visible, individual beads can still be wellresolved. Scale bar 10 μm in (**d-g**).

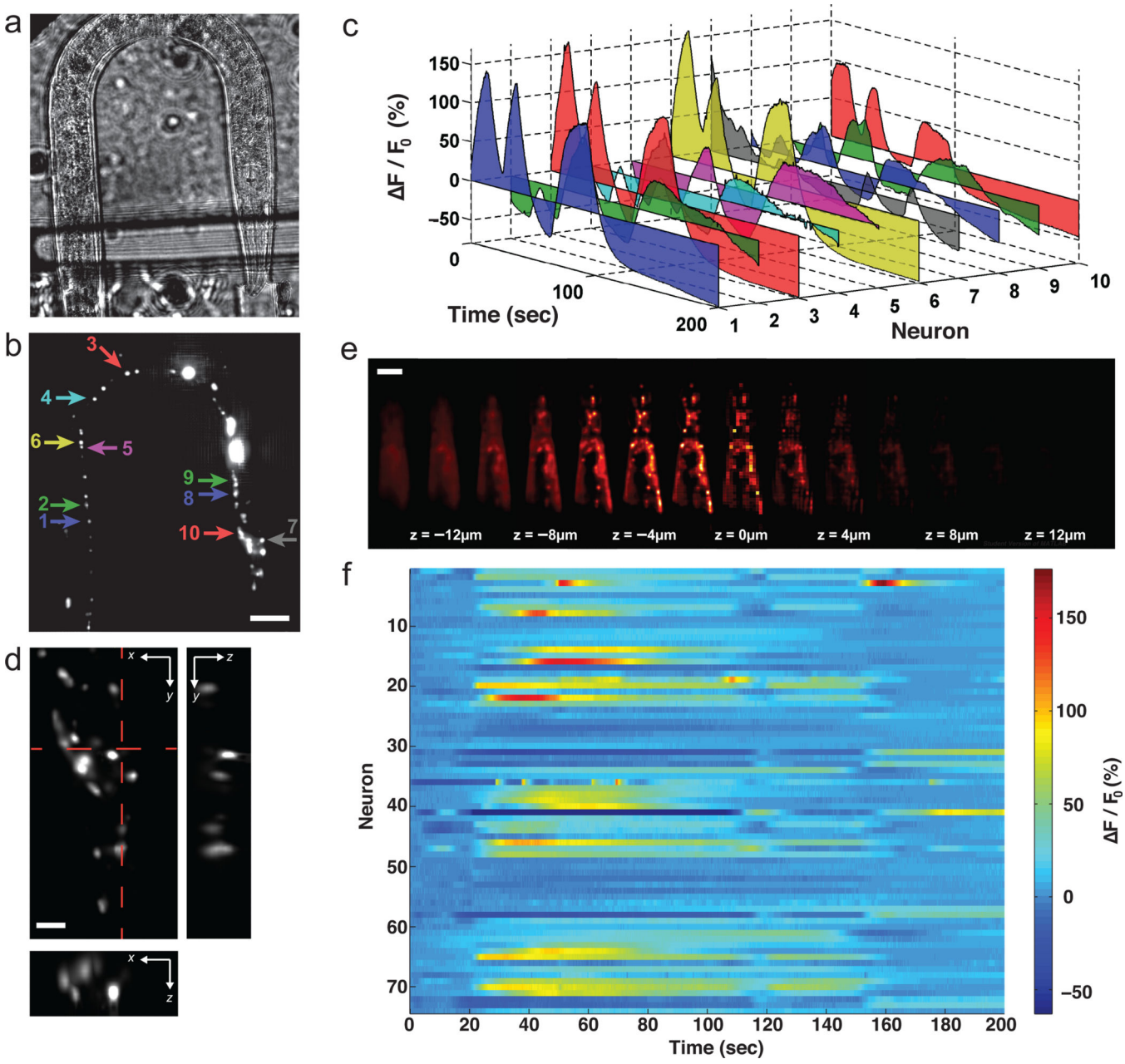

Figure 2.

Whole animal Ca^{2+}-imaging of *Caenorhabditis* elegans using light-fieldmicroscopy. (**a**) Wide-field image of the worm inside a microfluidicpoly(dimethylsiloxane) (PDMS) device used to immobilize the worm. Head is atbottom right. (**b**) Maximum intensity projection (MIP) of light-field deconvolvedimage (15 iterations) containing 14 distinct *z*-planes. The majority of the wormand its nervous system are clearly visible, including the head ganglia (at bottomright) as well as the ventral cord. Scale bar 50 µm. (**c**) Ca^{2+}-intensity traces($\Delta F/F_0$) of NLS-GCaMP5K fluorescence of selected neurons in the ventral cordand head region, as indicated by colored arrows and numbers in (**b**), and imagedvolumetrically at 5 Hz for 200 seconds. Also see **Supplementary Video 1.** (**d**)Zoom of the brain region,

with MIP of xy plane as well as *xz* and *yz* cross-sections indicated by the dashed lines. Single neurons are well resolved (**Supplementary Video 2**). Scale bar 10 μm. (**e**) Individual *z* planes of typical recording of theworm's brain, reconstructed from a single camera exposure (see also **Supplementary Fig. 2** for neuron IDs). In this recording, the worm's center wasplaced at the focal plane of the objective. Scale bar 50 μm. (*f*) Activity of all 74neurons identified in (**e**), also see **Supplementary Video 4**. Each row shows atime-series heat map. Color indicates percent fluorescence changes ($\Delta F/F_0$);scaling is indicated by the color bar on the right. The x-axis in (**f**) representselapsed recording time while the y axis shows individual neurons.

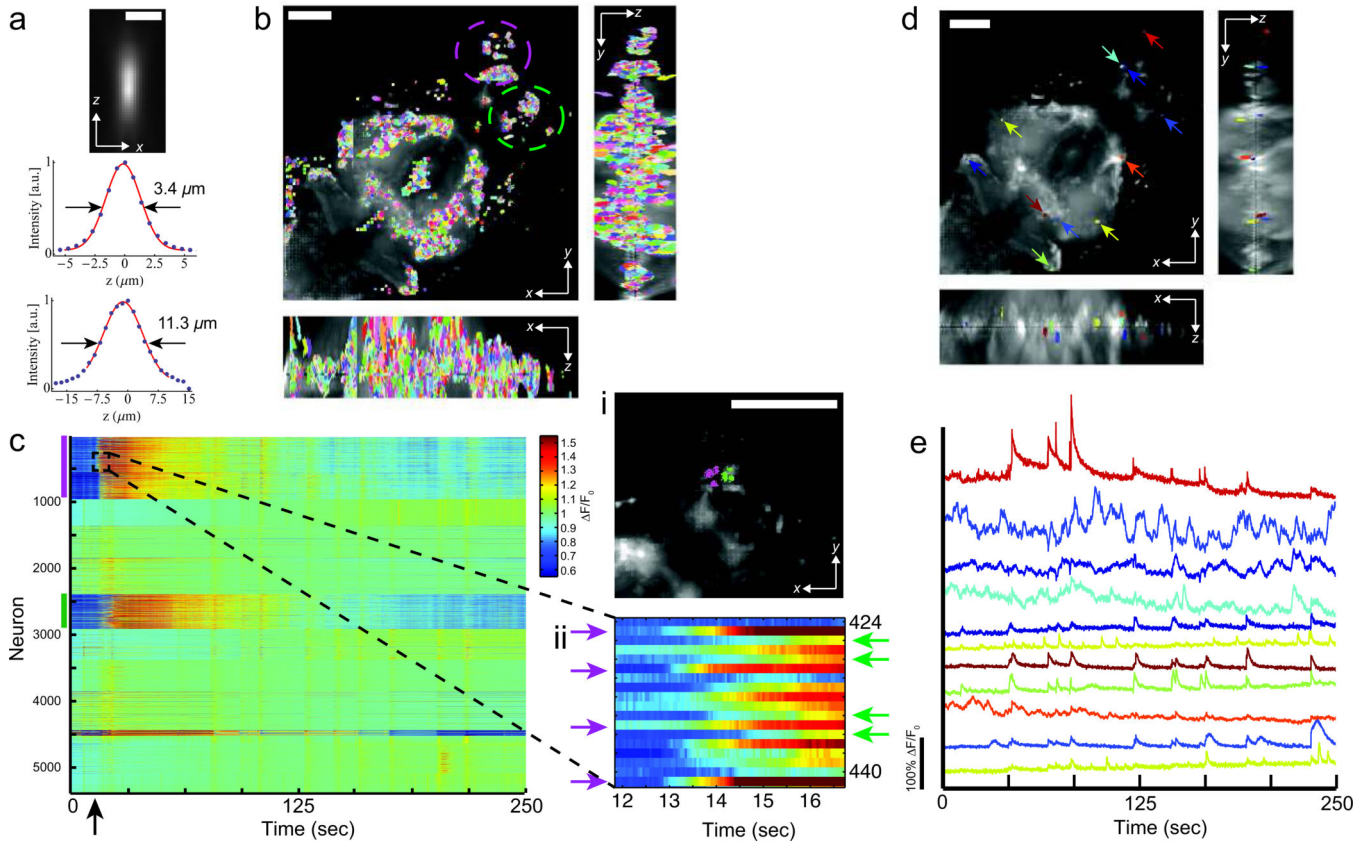

Figure 3.

Whole-brain Ca^{2+}-imaging of larval zebrafish brains in vivo.(**a**) Axial point spread function (PSF) of a 0.5 μm sized bead located at *z* = 28 μm off the focal plane for the 20× 0.5NA lens and corresponding x and z-profiles.Scale bar 10 μm. (**b**) Maximum intensity projection (MIP) of light-fielddeconvolved volume (8 iterations) containing 51 distinct z planes, captured at 50ms per frame exposure time and spaced 4 μm apart, showing *xy* plane, *xz* and *yz* cross-sections. Spatial filters, each representing individual cells, identified using PCA/ICA analysis [20] are shown. (**c**) Extracted Ca^{2+}-intensity signal ($\Delta F/F_0$)of GCaMP5 fluorescence using spatial filters shown in (**b**). Each row shows atime-series heat map with color indicating percent fluorescence changes ($\Delta F/F_0$).In total, 5,379 filters were automatically identified most of which correspond toindividual neurons. Color bars denote encircled regions in (**b**), which includeolfactory epithelium, olfactory bulb and telencephalon. At ~15 sec (denoted bythe arrow), decomposed fish water (an intrinsically aversive odor) was added tothe recording chamber evoking activity in the olfactory system. (**c i, ii**) Zoom-inof the dashed area in (**c**) showing individual Ca^{2+}-traces and their dynamicsimmediately following odor stimulation. The high time-resolution reveals subtle differences in the exact timing of the onset of the response for different spatial filters. Groups of cells constituting of neurons all within similar spatial proximitycan be observed (**c i**). While the neurons in each group exhibit a nearly synchronous onset of their activity, the collective response of each group isdelayed with respect to the others. (**d**) Overlay of MIP with randomly selectedspatial filters. (**e**) Ca^{2+}-intensity traces of selected cells shown in (**d**). Neuronswere manually selected from the olfactory system, midbrain and hindbrain.Trace

color matches spatial filter color in (**d**). Scale bar is 100 μm in (**b**), (**d**) and(**e**). Also see **Supplementary Video 6.**